

Quantized Repetitions of the Cuprate Pseudogap Line

Vincent Sacksteder IV*

Department of Physics, Royal Holloway University of London, United Kingdom

The cuprate high T_c superconductors exhibit a poorly understood pseudogap transition temperature which persists far above T_c , decreases as the material composition is doped to produce hole charge carriers, and traces a line across the temperature-doping phase diagram. We report a meta-analysis of all measurements of the pseudogap temperature in two prototypical cuprates, which reveals that the best known pseudogap line is one of a family of four lines. These lines all originate from a single point near one edge of the superconducting phase, and their slopes follow a quantized mathematical pattern. The pseudogap family suggests that the cuprates host a single mother phase and that the pseudogap lines, charge density wave order, and superconductivity are all subsidiary effects supported by the mother phase.

The cuprate high T_c superconductors are built from copper oxide planes, and when these planes are doped with holes superconductivity occurs. Temperatures above the superconducting critical temperature T_c make the cuprates effectively two dimensional by disrupting the weak interplane coupling. Nonetheless the cuprates exhibit a wide variety of mysterious features at temperatures far exceeding T_c . One of the first to be noticed is a broad peak in the magnetic susceptibility at a temperature T_{max} , which is accompanied by qualitative changes in electrical and thermal transport.^{1,2} At low dopings T_{max} reaches temperatures as high as 700 K, and it decreases linearly as the parent compound is doped with holes. Focus has since shifted toward a pseudogap temperature T^* which is substantially smaller than T_{max} and again decreases linearly with hole doping. T^* marks a depletion in the density of states, and has been measured by many experimental techniques including angularly resolved photoemission spectroscopy (ARPES).^{3,4} Over the years a perplexing cornucopia of other doping-dependent signals have been identified, including a lower pseudogap temperature T_ν , charge density waves, nematic order, and a linear resistance extending to very high temperatures marking the "strange metal" regime.^{5,6}

In this paper we identify an unexpected regularity in the cuprate phase diagram: four of the experimentally measured doping-dependent temperatures, including T_{max} , the pseudogap temperature T^* , and the lower pseudogap line T_ν , belong to a family which radiates from a common intersection and has slopes determined by a quantization rule. Our results are based on a comprehensive survey of research papers which report temperature scales well above T_c . The temperatures gathered here were all realized experimentally rather than by extrapolation from lower temperatures, and clearly identifiable signals occurred at the reported temperatures, including peaks, kinks, extinction of diffraction peaks, etc. In the interest of clarity we do not rely on universality arguments, and therefore restrict ourselves to two specific compounds ($\text{La}_{2-x}\text{Sr}_x\text{CuO}_4$ (LSCO) and $\text{YBa}_2\text{Cu}_3\text{O}_{6+\delta}$ (YBCO)), to two specific doping techniques (strontium doping for LSCO and oxygen doping for YBCO), and we

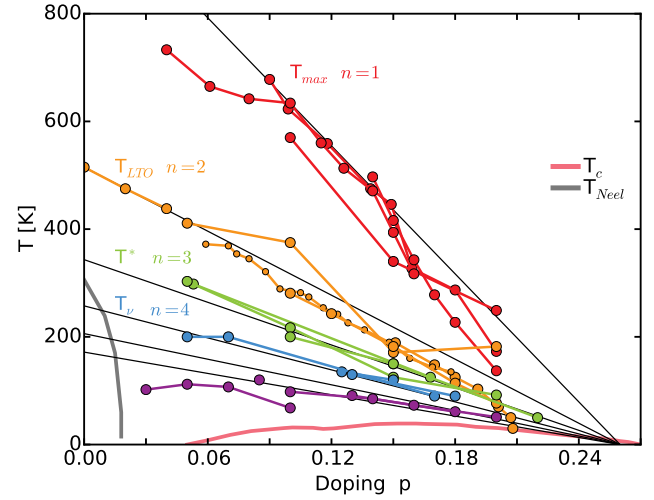


FIG. 1: (Color online.) The family of pseudogap lines in LSCO. The black guides to the eye have slopes proportional to $1/n$ and meet at doping $p = 0.26$. Individual pseudogap data sets, each from a distinct experimental group measuring a distinct experimental probe and signature, are shown as filled circles connected by lines. The hallmark of the first (red) pseudogap line T_{max} is a peak in the magnetic susceptibility. C_4 symmetry is broken on the second (orange) line T_{LTO} , and the ARPES density of states develops a pseudogap on the third (green) line T^* . The fourth pseudogap line T_ν (blue) is marked by transport signatures. Purple lines show NMR, Hall angle, heat capacity, and neutron scattering data sets. The pink line shows the superconducting T_c . An antiferromagnetic phase (grey line) is found at low dopings.

keep separate the results of distinct experimental groups and of distinct experimental probes and signatures. Full details about each data set and about our selection criteria are included in the supporting material.

LSCO data: Figure 1 summarizes the experimental corpus on LSCO. While this compound has a relatively low maximum T_c of about 39 K, it is stable up to 1000 Kelvin and the full range of dopings across the cuprate superconducting dome can be explored. In order to show the slope and profile of individual data sets we plot lines

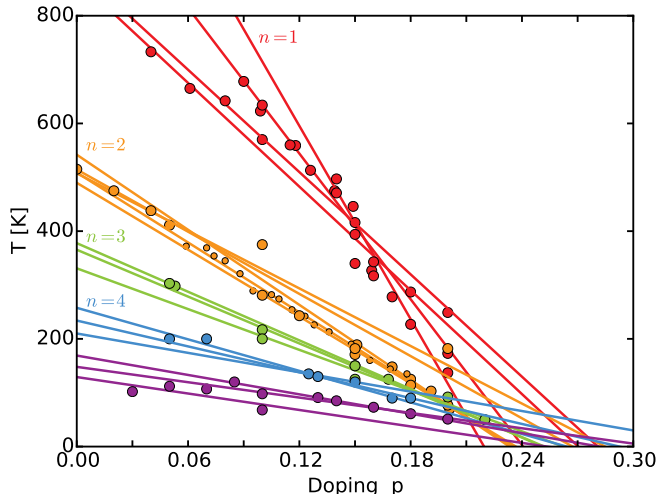


FIG. 2: (Color online.) Intersection of the pseudogap family in LSCO near $T = 0$, $p = 0.26$. The straight lines show linear fits to individual pseudogap data sets, displayed as filled circles.

connecting the data points within each set. All data sets are in agreement, showing clearly four characteristic temperatures. The topmost red lines show T_{max} , visible both as a peak in the magnetic susceptibility and as kinks in the resistance and thermoelectric power (TEP).^{2,7,8} The yellow lines (second from the top) show the temperature T_{LTO} of the well-known transition from the high symmetry tetragonal phase to a lower symmetry orthorhombic phase, which has generally though not unanimously⁹ been regarded as simply a structural phase transition with little relation to high T_c .⁸⁻¹² This transition manifests clearly in diffraction, resistance, and TEP measurements. The green lines (third from the top) mark the pseudogap temperature T^* , where ARPES shows that a pseudogap opens in the density of states. Like T_{max} and T_{LTO} , T^* is seen also in the resistance and the TEP.^{8,10,13-15} The blue lines (fourth from the top) are a recently identified second pseudogap transition T_ν , visible in the Nernst effect and in nuclear magnetic resonance (NMR).¹⁶⁻²⁰ This transition is well attested by Nernst and resistance measurements in Neodymium-doped and Europium-doped variants of LSCO, which give temperatures that agree very well with the LSCO data.^{17,21} We include also a few NMR, Hall angle, heat capacity, and neutron scattering data sets (in purple) which suggest similar lines at lower temperatures.^{20,22-24}

The four characteristic temperatures just discussed follow a pattern which we have highlighted with thin black lines.¹⁰² Both the experimental data and the black lines are organized as harmonics of the uppermost line, with the n -th line having a slope equal to $1/n$ times that of the highest $n = 1$ line. Moreover all four lines radiate from a point $p \approx 0.26$ that lies near the high-doping limit $p_{c2} = 0.27$ ²⁵ of the superconducting dome. Figure

2 displays linear regressions of each pseudogap data set. The linear regressions of fourteen out of eighteen pseudogap data sets intercept the $T = 0$ axis in the interval $p = [0.23, 0.29]$, of which six lie in $[0.25, 0.27]$.

Both the agreement of intercepts and the pattern of $1/n$ slopes are remarkable given that we have used very broad selection criteria embracing an extremely diverse set of experimental techniques and sample preparation protocols, publications from from 1990 to the present, and significant scatter within individual data sets. While it is often suggested that the pseudogap temperature is sensitive to the experimental technique, we find instead that all published measurements agree on the same simple pattern.

These results force the conclusion that all four characteristic temperatures are members of the same family. This family pervades most if not all of the cuprate phase diagram: in LSCO the $n = 2$ pseudogap line, i.e. the transition to orthorhombic symmetry, persists to zero doping and 515 K, and the $n = 1$ pseudogap line extends to above 700 K. Since the $n = 1$, $n = 3$, and $n = 4$ lines in this family are not structural transitions, the tetragonal to orthorhombic structural symmetry breaking on the $n = 2$ line must be a subsidiary signal of underlying electronic nematic order.

YBCO data: Figure 3 summarizes the experimental data on oxygen doped YBCO. Although this material has a considerably higher maximum $T_c \approx 94$ K, the data on its phase diagram is much curtailed. Hole dopings above $p = 0.194$ cannot be obtained at ambient pressure, and the experimental literature on the pseudogap generally has not measured dopings less than $p \leq 0.05$, most likely because of proximity to the antiferromagnetic Neel phase, marked in grey in Figure 3. Whether this practice assumes or confirms that the pseudogap lines do not coexist with Neel order seems unclear. In the remaining doping range $0.06 \leq p \leq 0.194$ we are able to clearly identify the $n = 2$, $n = 3$, and $n = 4$ pseudogap lines, which follow rays intersecting near $p \approx 0.215$.¹⁰³ The scatter around $p \approx 0.215$ is again notably small, comparable to the scatter around LSCO's $p \approx 0.26$. Figure 4 shows that the linear regressions of fifteen out of twenty-two pseudogap data sets intercept the $T = 0$ axis in the interval $p = [0.20, 0.24]$, and that six are clustered in $[0.21, 0.22]$.

YBCO shows again the same pattern of $1/n$ slopes seen in LSCO. The $n = 2$ (orange) line is YBCO's pseudogap temperature T^* , marked by transport signatures and the onset of fluctuating intra unit cell order. Recent symmetry-oriented experiments show that this is a nematic C_4 symmetry breaking transition similar to the symmetry breaking seen on LSCO's $n = 2$ line. However these experiments go beyond the diffraction experiments performed on LSCO, and find that C_2 , mirror, and inversion symmetries are also broken in addition to C_4 symmetry breaking.^{10,17,26-41} On the $n = 3$ (green) line T_{nem} , whose slope is $2/3$ of the pseudogap's slope, transport becomes nematic and time reversal symmetry is broken.^{10,42-45} The $n = 4$ (blue) T^{**} line has been

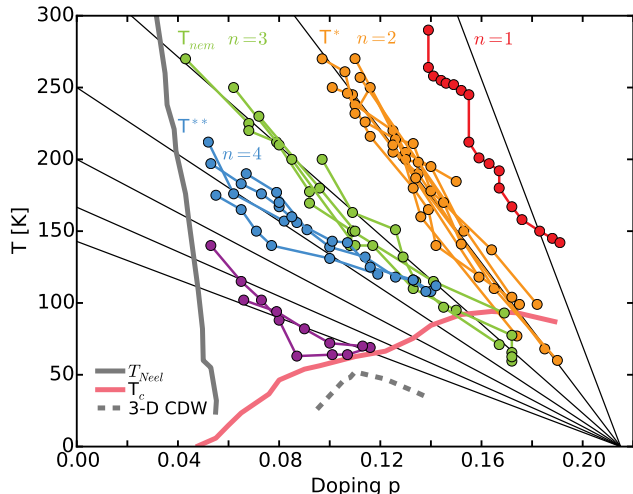


FIG. 3: (Color online.) The family of pseudogap lines in YBCO. The black guides to the eye have slopes proportional to $1/n$ and meet at doping $p = 0.215$. Individual pseudogap data sets, each from a distinct experimental group measuring a distinct experimental probe and signature, are shown as filled circles connected by lines. Near the first $n = 1$ pseudogap line a transport anomaly (red data set) occurs. C_4 and intra unit cell symmetries are broken on the second (orange) line T^* , while on the third (green) line T_{nem} transport becomes nematic and time reversal symmetry is broken. The fourth pseudogap line T^{**} (blue) is marked by transport signatures. Purple lines show additional transport data sets. The pink line shows the superconducting T_c . Underneath T_c three-dimensional charge density wave order (dashed grey) occurs, and an antiferromagnetic phase (solid grey) is found at low dopings.

measured in resistance and Hall resistance experiments, and its slope is $1/2$ of the pseudogap's slope.^{36,46,47} At dopings $p < 0.085$ intra unit cell ordering occurs on this $n = 4$ pseudogap line rather than on the $n = 2$ line.⁴⁸⁻⁵⁰

Turning to YBCO's $n = 1$ pseudogap line, experiments have almost never explored temperatures above 300 K because of concerns about thermal history memory, aging and equilibration, and preparation protocol. This leaves only a small corner in the phase diagram where the $n = 1$ line might be seen, stretching from $p = 0.15$, $T = 300$ K to $p = 0.194$, $T = 95$ K, which limits our ability to ascertain the existence of a line here. In this region there is a large step change in the resistance and an onset of thermal history memory^{51,52}. Moreover Ando's resistance measurements show a prominent white contour, plotted in red in Figure 3, which is roughly aligned with the expected $n = 1$ line.¹⁰

Comparison: Comparing LSCO to YBCO, the pseudogap lines extrapolate to zero-doping temperatures which are the same within experimental error, i.e. 515 K for LSCO's $n = 2$ line vs. 500 K for YBCO.¹⁰⁴ However the pseudogap family's meeting point on the $T = 0$ axis lies at considerably different dopings: in YBCO it

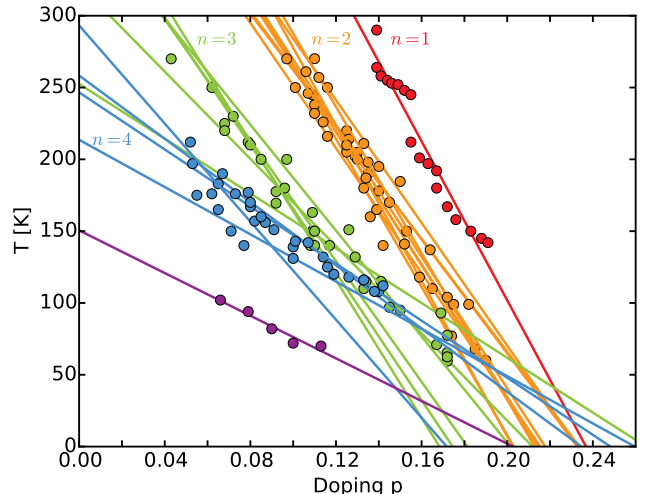


FIG. 4: (Color online.) Intersection of the pseudogap family in YBCO near $T = 0$, $p = 0.215$. The straight lines show linear fits to individual pseudogap data sets, displayed as filled circles.

lies at $p \approx 0.215$, while in LSCO it is found at $p \approx 0.26$. This should lay to rest debates over whether the pseudogap line intersects the superconducting dome or instead merges with T_c , and about the location of the putative quantum critical point: if the question is framed in terms of hole doping p , the answer clearly depends on the material. Yet the question can be answered in a different way that is not material dependent: in both LSCO and YBCO the intersection points lie very near to the maximal doping p_{c2} at which superconductivity can be achieved, which has two different values, $p_{c2} = 0.27$ ²⁵ in LSCO vs. $p_{c2} = 0.194$ ⁵³ in oxygen-doped YBCO at ambient pressure. In this sense the pseudogap lines in both LSCO and YBCO intersect at the real material-dependent end of the superconducting phase. We conclude that in both materials the entire superconducting dome lives under the shelter of the pseudogap family, and that its overdoped edge is tied to the pseudogap.

The various observables marking the pseudogap family collapse at critical dopings which depend on the line, and the doping scheme²¹, and the observable. On LSCO's $n = 1$ line the linear resistance signature collapses between $p = 0.17$ and $p = 0.18$ ^{7,17,54}, while the peak in the magnetic susceptibility continues past $p = 0.20$ ⁷. On the $n = 2$ line the tetragonal phase associated with this line collapses near $p = 0.208$ ⁹, and on the $n = 3$ line the ARPES pseudogap persists until at least $p = 0.22$ ¹⁴. It seems likely that the collapse of each line is caused by a small competing temperature scale, since in both LSCO and YBCO the $n = 2$, $n = 3$, and $n = 4$ lines either collapse or disappear from the experimental record between 50 and 110 K. The coupling between copper oxygen planes is a likely candidate for supplying the competing scale, since it supports long range 3-D charge density

waves and superconductivity in roughly the same temperature range.

The signatures of the pseudogap lines in YBCO may differ substantially from those in LSCO. Except for the $n = 2$ line, comparisons of symmetry breaking are impossible because LSCO pseudogap experiments have generally not probed symmetry breaking. Moreover, the hallmark of LSCO's $n = 3$ line is that the ARPES density of states begins to manifest a pseudogap. Since there is no ARPES data on YBCO's pseudogap temperature, in YBCO the same change in the density of states could occur on the same $n = 3$ line. However this change is generally believed to occur instead on YBCO's "pseudogap line" i.e. its $n = 2$ line. This question is confused further by data on $p \approx 0.14$ $\text{Bi}_2\text{Sr}_2\text{CaCu}_2\text{O}_{8+\delta}$ (Bi2212) where the ARPES pseudogap seems to open in two discrete steps near $T = 250$ K and $T = 150$ K, suggesting that in Bi2212 the density of states may change substantially at two distinct pseudogap lines.⁴

Analysis: These results are very fertile ground. First, the fact that the pseudogap family spans all dopings up to p_{c2} and temperatures up to 700 K argues strongly that the entire phase diagram up to p_{c2} hosts a single mother phase or order. The various phenomena observed along the pseudogap lines, for instance the structural phase transition to orthorhombic order, are then subsidiary or parasitic phenomena that respond to underlying changes in the mother phase. The details of which line a particular observable (such as orthorhombic symmetry) is associated with may depend on the material, and even when a particular observable in a particular material collapses at a particular doping the underlying line in the mother phase may continue robustly to higher dopings. As a case in point, in YBCO intra unit cell order switches from the $n = 4$ line to the $n = 2$ line near $p = 0.085$ ^{31-34,37,48-50}, while transport signals show that the $n = 4$ line continues until at least $p = 0.142$.^{36,46,47} Superconductivity may also be a subsidiary or parasitic phenomenon which occurs when (a) the mother phase assists hole transport and (b) the interlayer coupling is strong enough to support long range 3-D order.

Secondly, the width of the pseudogap lines is unquestionably sharp compared to the pseudogap temperatures themselves. Figures 1 and 3 show that the scatter around each pseudogap line is typically of order ± 15 K.¹⁰⁵ This sharpness could be understood as evidence of standard phase transitions. However the fact that there is a family of repeated pseudogap lines indicates that we are instead seeing a quantum coherent effect in the mother phase, in the same category as Landau levels or atomic orbitals. If so, then quantum coherence must persist to temperatures as high as 700 K in the cuprates. This conclusion is reinforced by parallel evidence from the strange metallic (linear in magnetic field and linear in temperature) resistance seen in the cuprates, which is also a manifestation of quantum coherence at temperatures far above T_c .⁵⁵⁻⁵⁷

Thirdly, the pseudogap lines are in truth linear. Clarity about this linearity was obtained by restricting our

data to single materials with a single doping scheme. There are some mild deviations from linearity - YBCO's $n = 4$ pseudogap line flattens at around 140 K, and LSCO's $n = 1$ and $n = 2$ lines steepen at high dopings - but these are mild distortions, and are the exception rather than the rule. The pseudogap lines relate temperature T to the 2-D sheet density of holes $\rho_{holes} = p/\mathcal{A}$ within the copper oxide plane. Here \mathcal{A} is the area of the copper oxide unit cell. Since in atomic units sheet density has the same units as both temperature and energy, we conclude that the pseudogap temperatures are direct measures of a sheet density. This conclusion is supported by the fact that the constant of proportionality between the $n = 1$ pseudogap line and ρ_{holes} is of order one: -1.27 for LSCO and -1.55 for YBCO. The natural endpoint of this reasoning is that in the cuprates there is a two dimensional sheet density Π_{psg} which controls both the pseudogap family and the family's mother phase, that $\Pi_{psg} \propto p_{c2} - p$ is high at low dopings and decreases linearly to zero at p_{c2} , and that the pseudogap temperatures are direct measures of this density.

Two other linear relations between sheet density and temperature have already been seen in the cuprates. Uemura's proportionality relation between the superfluid density and T_c holds in many underdoped materials⁵⁸, and a formally identical relation has been verified also in overdoped LSCO⁵⁹. Secondly, several LSCO and Bi2212 experiments have reported temperature scales which rise linearly with hole doping p and extrapolate to zero at the underdoped end of the superconducting dome, so that these temperatures seem to measure the sheet density of mobile holes - see Figure 6 in the supporting material for a summary of these results.^{8,60-62} It is also significant that 3-D long range charge density wave (CDW) order and the 1/8-th anomaly occur near half-filling for Π_{psg} , suggesting that these may be favored when the pseudogap density is about one half of its maximum value.

It is technically possible that the pseudogap density Π_{psg} and pseudogap lines could reflect strictly ultraviolet i.e. short range physics near the atomic scale, and that the cuprate phase diagram is not controlled directly by Π_{psg} but instead through renormalization group flow. This has the weaknesses that atomic scale physics would be expected to cause resonances in the phase diagram at values of Π_{psg} tied to the crystal structure, but these are not seen, and that at dopings near p_{c2} the area scale indicated by Π_{psg}^{-1} is far in excess of the atomic scale. In our view it is more likely that Π_{psg} is a fundamental determining property of long-range order in the pseudogap mother phase. We leave for future work the question of what quantity is counted by Π_{psg} , although some of the obvious possibilities are vortices, skyrmions, dislocations, entanglement density, or topological quantities.

Fourthly, we turn to the $1/n$ quantization rule which controls the slopes. In this connection we are inspired by recent experimental and theoretical work which shows a direct linear relation between magnetic field B and temperature T in the strange metal phase of LSCO and other

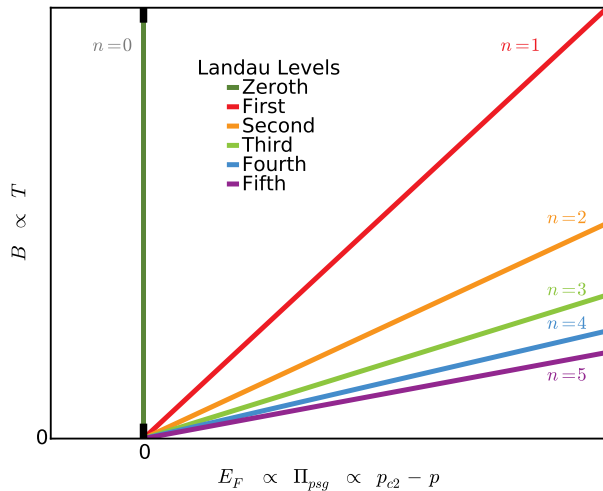


FIG. 5: (Color online.) Effective model producing the same pattern seen in the pseudogap family. The model describes free two-dimensional $p^2/2m_e$ fermions with a Zeeman splitting $\mu_0 B \sigma_z$ moving in a magnetic field B . We plot the resulting Landau levels with their energies E_n along the x axis and with magnetic field B along the y axis. The Landau level slopes follow the same $1/n$ pattern seen in the pseudogap family if field B is mapped to temperature and Fermi energy E_F is mapped to pseudogap density Π_{psg} .

bad metals.^{55–57,63} The pattern traced by the pseudogap family can be reproduced by a model of free two dimensional $p^2/2m$ fermions where temperature is mapped to an effective magnetic field B and the pseudogap sheet density $\Pi_{psg} \propto p_{c2} - p$ is mapped to a Fermi level E_F . As shown in Figure 5, if the effective model includes either a Berry phase⁶⁴ or a Zeeman term $\mu_0 B \sigma_z$, then its Landau levels have the same $1/n$ slopes seen in the pseudogap family and intersect at a common point $B = 0$, $E_F = 0$. This model leads us to the conjecture that the pseudogap family is in some way related to the Integer Quantum Hall Effect. Our conjecture is not a suggestion of well-defined quasiparticles or, going further, a Fermi liquid or band structure. Topology can control conduction even when these concepts are not relevant, as has been seen in studies of strongly disordered topological insulators.⁶⁵

Figure 5 shows that the effective model possesses an additional $n = 0$ Landau level at $E_F = 0$, which maps to a vertical line in the cuprate phase diagram at the upper critical doping p_{c2} . This prediction is confirmed in LSCO by three experimental signatures which are extinguished on this line: the superfluid density⁵⁹, the electronic nematicity which is found at all lower dopings⁶⁶, and the coefficient of the linear-in-temperature contribution to the resistivity^{25,67}.

In summary, we have argued that the entire cuprate phase diagram from zero doping out to p_{c2} hosts a single mother phase which is controlled by a two dimensional sheet density, and that the observed family of pseudogap

lines are subsidiary phenomena caused by changes in the mother phase. We also suggest that the superconducting phase and charge density wave order are supported by the mother phase and occur when it is augmented with an interplane coupling and, in the case of superconductivity, with hole carriers.

Acknowledgments

We gratefully acknowledge stimulating discussions with K. S. Kim, J. Zaanen, A. Ho, S. Hayden, M. Surlangi, K. Schalm, V. Cheianov, T. Ziman, I. Vishik, J. Saunders, and especially A. Petrovic. We thank the Instituut Lorentz in Leiden for hospitality, and the Hubbard Consortium for facilitating discussions. We acknowledge support from EPSRC grant EP/M011038/1.

Appendix A: Temperature scales that rise proportionally to hole doping

With the exception of Refs. 68,69, the data sets graphed in Figure 6 are temperatures that rise linearly with doping and extrapolate to $T = 0$ near the underdoped limit of the superconducting dome, i.e. in the interval $p = [0.049, 0.081]$. This suggests that these temperatures are direct manifestations of the sheet density of mobile holes. Ref. 68 reports an energy scale with a similar behavior.

Ref. 69 also reports a temperature which rises linearly up to $T = 300$ K. This last data set extrapolates to $T = 0$ at a lower doping $p = 0.023$, presumably because of a sensitivity to pinned holes.

All data sets used in Figure 6, with discussion of their particulars and origin, and with a script that produces this figure, are available in the supporting material as a python script.

1. Hashimoto, 2009.⁶¹ Angularly integrated ARPES. LSCO. The authors take the first derivative of the spectrum with respect to energy, and identify a peak in the first derivative. The temperature reported here, which they call a coherence temperature, is a break in the temperature dependence of the peak position. We omit a data point at $p = 0.15$ which fits well with the linear regression because they did not actually reach the reported temperature $T = 364$ K. Roughly consistent with Ref. 68. The slope is 6200 K without the $p = 0.15$ data point, or 4900 K with it.
2. Ino, 2009.⁶⁸ Angularly integrated ARPES. LSCO. The quantity reported here is a measure of the width of the Fermi surface. Unlike all other data discussed in this article, this is an energy scale converted to temperature, not an experimental temperature. The experiment was performed at $T = 18$ K. The quantity reported here includes a factor of

$1/\pi$ which might be able to be renormalized at will. We include this data set because the four data points between $p = 0.074$ and $p = 0.203$ rise linearly with doping and extrapolate to the underdoped edge of the superconducting dome. We omit the $p = 0.30$ point from the linear fit, and we omit the $p = 0$ point altogether because Figure 2 in Ref. 68 shows $p = 0$ data that seems to leave little ground for extracting a width. The slope is 4600 K.

3. Kim, 2004.⁸ Thermoelectric power. LSCO. The temperature reported here marks a break from the linear signal seen at high temperatures. Here we plot only the dopings at $p = 0.20$ and higher. The slope is 2100 K, about half of the slope in Ref. 68.
4. Chatterjee, 2011.⁶² ARPES. Bi2212. Below this temperature the spectrum contains a sharp Gaussian peak, and above this temperature the peak is absent. Unlike all other data discussed in this article, this data is obtained from Bi2212.
5. Kim, 2004.⁸ Thermoelectric power. LSCO. The temperature reported here marks a break from the linear signal seen at low temperatures. Here we plot only the dopings at $p = 0.20$ and higher.
6. Ohsugi, 1991.⁶⁰ Nuclear quadrupole resonance. LSCO. The temperature reported here is a Weiss temperature obtained by fitting the nuclear spin relaxation rate to a Curie-Weiss law.
7. Panagopoulos, 2006.⁶⁹ See also Ref. 70 by the same group. LSCO. This temperature marks the onset of hysteresis in the temperature dependence of the low field magnetization, which is probably a sign of pinned vortices and of pairing. The low-doping data from $p = 0.03$ to $p = 0.10$ nicely follows a straight line originating at $T = 0$, $p = 0.023$ and extending up to room temperature. The small $p = 0.023$ intercept may be caused by the observable's sensitivity to both pinned and mobile holes. The slope is about 3900 K, roughly comparable to the slopes of the LSCO ARPES data sets.^{61,68}

Appendix B: LSCO Data Sets

The temperatures gathered here were all realized experimentally rather than by extrapolation from lower temperatures, and clearly identifiable signals occurred at the reported temperatures, including peaks, kinks, extinction of diffraction peaks, etc. In the interest of clarity we do not rely on universality arguments, and therefore restrict ourselves to lanthanum cuprate with strontium doping (LSCO), and we keep separate the results of distinct experimental groups and of distinct experimental

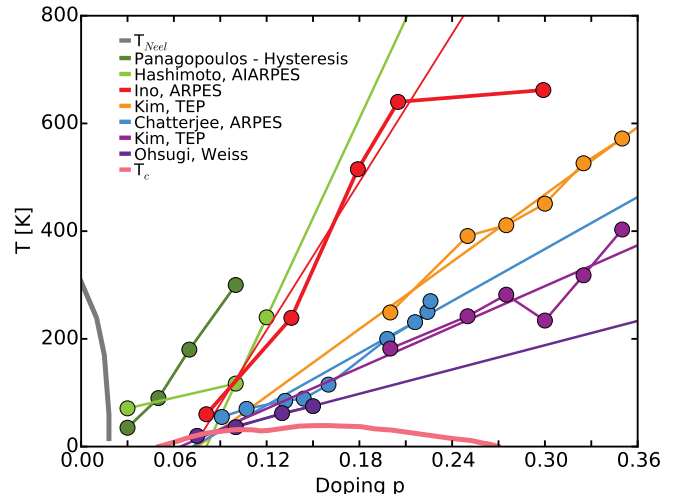


FIG. 6: (Color online.) Characteristic temperatures that seem to be direct manifestations of the density of mobile holes. Light green, red, and blue data sets were measured using ARPES, yellow and light purple sets with the thermoelectric power, and the dark purple data set with the magnetic susceptibility. The dark green set measuring the onset of magnetic hysteresis intercepts the p axis at lower doping, perhaps because it is sensitive to pinned holes. The superconducting dome is shown in pink, and the antiferromagnetic phase in grey.

probes and signatures. We do not report any temperatures that are not already reported by the articles we have cited. In particular, we have stayed out of the business of re-analyzing or fitting data sets from other articles. The one exception to this rule is our use of the color maps in¹⁰ - from that article we extracted data from certain contours and features that are prominent in the color maps.

Our survey of pseudogap temperature measurements does not extend to the extensive literature on anomalies and phase transitions measured using mechanically-oriented observables such as internal friction, sound velocity, lattice constants, thermal expansivity, and the like.⁷¹

All data sets used in the LSCO figures or enumerated here, with discussion of their particulars and origin, and with a script that produces the figures, are available in the supporting material as a python script.

1. $n = 1$ line: In LSCO the $n = 1$ line marks a resonance in the magnetic susceptibility and qualitative changes in transport and in the thermoelectric power.
 - (a) Yoshizaki, 1990.² Peak in the magnetic susceptibility.
 - (b) Nakano, 1994.⁷ Peak in the magnetic susceptibility. The peak disappears near $p = 0.22$. We omit the last three data points because

no peak exists in those susceptibility curves until a Curie term has been subtracted. We also omit the first four data points, at lowest doping, because the experimental temperature did not go high enough to see the actual peak. The scaling analysis used to obtain those four points is however very convincing, especially because the peak was seen at lower dopings by².

- (c) Kim, 2004.⁸ Thermoelectric power. The temperature reported here marks a break from the linear signal seen at high temperatures. Here we plot only the dopings up to $p = 0.20$.
- (d) Nakano, 1994.⁷ Resistivity. The temperature reported here marks a break from the linear signal seen at high temperatures. The break disappears and the signal seems to be perfectly linear (from visual inspection) at $p = 0.16$ and $p = 0.18$, which is consistent with Ref. 54's data at $p = 0.17, 0.18$. This is also consistent with Ref. 17's statement that the resistivity signal of the pseudogap collapses between $p = 0.17$ and $p = 0.18$.

There is apparent disagreement between Ref. 7 and Ref. 72, which was cited by Ref. 17 by the same authors. Ref. 7 reports that at $p = 0.14$ and $p = 0.16$ the pseudogap temperature, i.e. the onset of linear in temperature resistance, occurs at 471 K and 317 K respectively. In contrast Ref. 72 gives resistivity data at $p = 0.136, 0.143, 0.157, 0.163$ that superficially indicates much smaller temperatures. The $p = 0.136$ resistivity seems to be linear above 150 K or so, and the $p = 0.143$ resistivity seems to be linear above 110 K. However Ref. 72's data goes up to only 200 K, so they are unable to detect any linearity above 471 K. In contrast, Ref. 7's data at $p = 0.14$ extends up to 900 K. Moreover, Ref. 7's data extends down to the superconducting temperature, shows that the slope below 471 K is not very different from the slope above that temperature, and changes only gradually. Therefore Ref. 72 may just not have enough data to detect nonlinearity near the high end of their temperature range. A second alternative is that there could be two linear regimes, one above 471 K, and another above 110 - 140 K, corresponding to two pseudogap temperatures.

- 2. $n = 2$ line: In LSCO the $n = 2$ line is a symmetry breaking transition from C_4 down to C_2 nematic order. It has been commonly regarded as a structural transition from tetragonal to orthorhombic symmetry. It is accompanied by features in transport and in the thermoelectric power.

- (a) Kim, 2004.⁸ Thermoelectric power. The temperature reported here marks a break from the linear signal seen at low temperatures.
 - (b) Takagi, 1992.⁹ X-ray diffraction, looking for a peak splitting caused by orthorhombicity. This data shows that the signal i.e. the orthorhombic phase collapses near $p = 0.208$. Our linear fit omits two points dropping almost vertically near $p=0.208$.
 - (c) Ando, 2004. Resistivity.¹⁰ We reproduce a red linear feature that is very prominent in Ando's plot. The feature disappears in the range between $p = 0.178$ and $p = 0.19$.
 - (d) Yamada, 1998.¹¹ Neutron scattering sensitive to orthorhombic symmetry.
 - (e) Keimer, 1992.¹² Neutron scattering sensitive to orthorhombic symmetry. More specifically, extinction of the (021) superlattice reflection peak.
- 3. $n = 3$ line: In LSCO the $n = 3$ line, also called the pseudogap temperature, is marked by the birth of a pseudogap controlling the density of states. It is accompanied by features in transport and in the thermoelectric power.
 - (a) Yoshida, 2012.¹³ ARPES. The data here is the temperature where the pseudogap (measured with ARPES) disappears.
 - (b) Ando, 2004.¹⁰ Resistivity. We reproduce a line segment imposed on the data by the authors which follows qualitative trends of the colors in their graph. We omit the first of the two line segments which they imposed, a constant-temperature $T = 298$ K line at low doping $p \leq 0.053$. This $T = 298$ K line is in fact supported by colors in the graph. At the overdoped end, the authors' line continues to $p = 0.168, T = 125$ K, but the underlying resistivity data suggests that the line should stop a little earlier, between $p = 0.15$ and $p = 0.168$.
 - (c) Kim, 2004.⁸ Peak in the thermoelectric power. Here we plot only the dopings from $p = 0.05$ up to $p = 0.20$. At higher dopings the signal increases very slowly with doping.
 - (d) Hashimoto, 2007.¹⁴ Angularly integrated ARPES. At temperatures below this temperature the density of states increases relatively rapidly with temperature, and above this temperature the DOS increases less quickly with temperature - i.e. the slope changes from one value to another in a discontinuous way. We omit a zero temperature data point at $p=0.30$ because it only bounds the doping value where this line collapses to the range between $p = 0.22$ and $p = 0.30$. We also omit the

$p = 0.03$, $T = 300$ K data point because here no break is observed in the data, i.e. there is no data above 300 K. This pseudogap temperature is based on the authors noticing that at other dopings the slope below T^* decreases inversely with T^* , as seen in the inset of their Figure 2a. This $p = 0.03$ data point agrees very well with all other data points on this line, and extends the line down to $p = 0.03$.

- (e) Matt, 2015.¹⁵ ARPES. Based on measurements of the normal-state antinodal spectral gap - T^* is the temperature where this gap goes to zero. This data point is omitted because it concerns Nd-LSCO, but it does match the $n = 3$ line well. They also show a strong pseudogap at $p = 0.12$ which results in a bound $T^* > 75$ K, though probably T^* is much larger than 75 K.
4. $n = 4$ line: In LSCO the $n = 4$ line is marked by features in transport and in nuclear magnetic resonance.

We plot only the first three data sets listed here. The same pseudogap line revealed by these three data sets is very well supported by resistivity and Nernst data from Nd-LSCO and Eu-LSCO, as documented in the remaining data sets. All resistivity and Nernst data sets are shown together in Ref. 17 and show impressive agreement.

- (a) Cyr-Chinoire, 2018 re-analyzes Fujii, 2010.^{16,17} Nernst effect. The temperature reported here marks a break from the linear signal seen at high temperatures.
- (b) Cyr-Chinoire, 2018 re-analyzes Ong, 2010/2011.¹⁷⁻¹⁹ Nernst effect. The temperature reported here marks a break from the linear signal seen at high temperatures. This data set is a re-analysis of Nernst effect data from two papers which have Wang, Xu, Ong, and Uchida as co-authors.
- (c) Itoh, 2004.²⁰ NMR. Peak in the nuclear spin-lattice relaxation rate.
- (d) Cyr-Choiniere, 2018.^{16,17,73} Nernst effect. The temperature reported here marks a break from the linear signal seen at higher temperatures. This data set of three data points from $p = 0.15$ to $p = 0.21$ is omitted because it concerns Nd-LSCO, but it matches the LSCO $n = 4$ line well. It includes one data point from Ref. 16. It also includes two data points from Cyr-Choiniere's Ref. 73. A third $p = 0.24$ data point from Cyr-Choiniere is not included in the data set (a double omission) because it lies at $T = 0$ and therefore it only bounds the doping value rather than fixing it - however this data point does show

that in Nd-LSCO this pseudogap line collapses somewhere between $p = 0.21$ and $p = 0.24$.

- (e) Collignon, 2017.²¹ Resistivity. The temperature reported here marks a break from the linear signal seen at higher temperatures. This data set from $p = 0.20$ to $p = 0.24$ is omitted because it concerns Nd-LSCO, but it matches the $n = 4$ line well. When fitting to a straight line, we (doubly) omit a $T = 0$ data point at $p = 0.24$. The pseudogap temperature at $p = 0.23$ is 40 K, so the pseudogap temperature collapses to zero between $p = 0.23$ and $p = 0.24$.
- (f) Collignon, 2017, analyzes Ichikawa, 2000.^{21,74} Resistivity. The temperature reported here marks a break from the linear signal seen at higher temperatures. This data set from $p = 0.12$ to $p = 0.15$ is omitted because it concerns Nd-LSCO, but it matches the $n = 4$ line well. This data set is two data points obtained by re-analyzing data from Ichikawa.
- (g) Cyr-Chinoire, 2018.^{17,73} Nernst effect. The temperature reported here marks a break from the linear signal seen at higher temperatures. This data set from $p = 0.08$ to $p = 0.21$ is omitted because it concerns Eu-LSCO, but it matches the LSCO $n = 4$ line well. One data point within this data set is obtained from re-analysis of work from separate authors, so we (doubly) omit it. Three data points are from Ref. 17 and one data point is from Ref. 73 by the same authors.

5. Other Data Sets:

- (a) Baledent, 2010.²² Neutron scattering detecting intra unit cell two-dimensional short range order. This data point lies 4K above the $n = 6$ line, well within experimental error bars.
- (b) Itoh, 2004.²⁰ NMR. A minimum in the nuclear spin-lattice relaxation rate. This data set looks like it could belong to the 5th or $n = 6$ line.
- (c) Xu, 2000.²³ Tangent of the Hall angle. The temperature reported here marks a break from a quadratic form which gives a good fit at higher temperatures. We omit a data point which lies at $T = 0$, $p = 0.17$ because it only bounds the doping value where this temperature goes to zero to the interval between $p = 0.10$ and $p = 0.17$.
- (d) Matsuzaki, 2004.²⁴ Peak in the heat capacity divided by temperature. This data set lies near the $n = 5$ and $n = 6$ lines.

6. Superconducting T_c and Neel temperature:

- (a) Momono, 1994.⁷⁵ T_c .

- (b) Ando, 2004.¹⁰ T_c .
- (c) Doiron-Leyraud, 2009.²⁵ $T_c = 0$ at $p = p_{c2} = 0.27$.
- (d) Keimer, 1992.⁷⁶ Neel temperature measured with neutron scattering.
- (e) Matsuda, 2002.⁷⁷ Neel temperature measured with neutron scattering.
- (f) Niedermayer, 1998.⁷⁸ Neel temperature measured with muon spin rotation.

7. Omitted Data Sets:

- (a) Panagopoulos, 2004, 2005, 2006.^{69,70,79} Onset of hysteresis in the temperature dependence in the low field magnetization. We omit these data sets because they are clearly not related to the pseudogap family. They look like a high-temperature replica of the superconducting dome, reaching a maximum $T \approx 300$ K, and cut across the $n = 2$ line and all lower lines.
- (b) Oda, 1990.⁸⁰ Peak in the magnetic susceptibility. We omit this data set because it seems to have been superseded by Ref. 7 by the same authors.
- (c) Oda, 1990.⁸¹ Peak in the magnetic susceptibility. We omit this data set because it duplicates data in Ref. 80 by the same authors.
- (d) Oda, 1991.⁸² Peak in the magnetic susceptibility. We omit this data set because it seems to have been superseded by Ref. 7 by the same authors. It does indicate that the peak disappears between $p = 0.19$ and $p = 0.21$.
- (e) Momono, 1996.⁸³ Peak in the magnetic susceptibility. We omit this data set because it seems to duplicate data in Ref. 7, which was published in the same year by the same authors.
- (f) Nakano, 1998.⁸⁴ Peak in the magnetic susceptibility. We omit this data set because five out of six data points are the same as Ref. 7 by the same authors, but divided by 4.3 in order to map to an energy scale.
- (g) Nakano, 1998.⁸⁴ Magnetic susceptibility. The temperature reported marks a break from the linear form seen at high temperatures. We omit this data set because it is the same as the susceptibility data in Ref. 7 by the same authors, divided by 4.3 in order to map to an energy scale.
- (h) Nakano, 1998.⁸⁴ Resistivity. We omit this data set because it is roughly a factor of six smaller than the resistivity data in Ref. 7 by the same authors. The authors probably divided this data by some number to map to an energy scale, just as they did with the magnetic susceptibility data.
- (i) Hwang, 1994.⁸⁵ Hall resistance. We omit this data set because the method used to obtain it seems to allow for renormalization of the entire data set by a somewhat arbitrary multiplicative factor.
- (j) Batlogg, 1994.⁸⁶ Hall resistance. We omit this data set because the method used to obtain it seems to allow for renormalization of the entire data set by a somewhat arbitrary multiplicative factor. The authors are the same as in Ref. 85 and the Hall resistance data looks the same too. However here the data are limited to $p = 0.15$ and higher while the other article includes five additional dopings that are less than $p = 0.15$.
- (k) Batlogg, 1994.⁸⁶ Reanalysis of Yoshizaki's magnetic susceptibility data, looking for a shoulder rather than a peak. We omit this data set because for the two highest doping data points the shoulder is hard to identify and because at the four lower doping data points the physical meaning of the shoulder is not clear, since it remains to be seen whether there is actually a peak at those dopings.
- (l) Batlogg, 1994.⁸⁶ Resistivity - "changes of the high temperature slope curves." We omit this data set because it is only at lower dopings and its mathematical and physical meanings are not clear.
- (m) Tallon, 1999, analyzes Boebinger, 1996.^{87,88} Resistivity. We omit this data set because the method used to obtain it seems to allow for renormalization of the entire data set by an arbitrary multiplicative factor.
- (n) Johnston, 1989.¹ Peak in the magnetic susceptibility. While this paper is distinguished by being perhaps the first to notice a spin pseudogap, only three data points concern strontium doped LSCO. Of these three points, only one is from data that actually showed a peak in the susceptibility. We omit the remaining data point.
- (o) Takemura, 2000, analyzes Nishikawa, 1994.^{89,90} Thermoelectric power, analyzed with a universal scaling method. We do not plot this data because the temperature reported here lies in the tail of the universal scaling curve and is not associated with any clear feature. On the other hand the results here are roughly the same as those produced by⁸'s thermoelectric power experiment, which used the onset of a linear signal to define their characteristic temperature.
- (p) Startseva, 1999.⁹¹ Optical reflectivity and conductivity. We omit this data because there are only two data points at dopings separated by

only 0.01 (probably close to the error bars in doping), and because the difference in temperature is very large: 50 K.

- (q) Wang, 2006.⁹² Nernst effect. The temperature reported here marks a break from the linear signal seen at higher temperatures. We omit this paper and several others by the same group because their data has recently been questioned and re-interpreted by Ref. 17.

Appendix C: YBCO Data Sets

The temperatures gathered here were all realized experimentally rather than by extrapolation from lower temperatures, and clearly identifiable signals occurred at the reported temperatures, including peaks, kinks, extinction of diffraction peaks, etc. In the interest of clarity we do not rely on universality arguments, and therefore restrict ourselves to oxygen doped YBCO, and we keep separate the results of distinct experimental groups and of distinct experimental probes and signatures. We do not report any temperatures that are not already reported by the articles we have cited. In particular, we have stayed out of the business of re-analyzing or fitting data sets from other articles. The one exception to this rule is our use of the color maps in Ref. 10 - from that article we extracted data from certain contours and features that are prominent in the color maps.

Our survey of pseudogap temperature measurements does not extend to the extensive literature on anomalies and phase transitions measured using mechanically-oriented observables such as internal friction, sound velocity, lattice constants, thermal expansivity, and the like.^{52,71} Nor did we explore the extensive literature on hysteresis in YBCO and associated onset temperatures, or on oxygen movement and ordering.

When the hole doping was not reported, we used Ref. 53 to map from oxygen content (or, in one case, from T_c) to hole doping.

All data sets used in the YBCO figures or enumerated here, with discussion of their particulars and origin, and with a script that produces the figures, are available in the supporting material as a python script.

1. $n = 1$ line:

- (a) Ando, 2004. Resistivity.¹⁰ We reproduce a white contour that is prominent in Ando's data and starts near $p = 0.140$, $T = 291$ K.

2. $n = 2$ line: In YBCO the $n = 2$ line is marked by broken C_4 , C_2 , mirror, and inversion symmetries, by fluctuating intra unit cell order which includes time reversal symmetry breaking, by a new contribution to nematic ordering, and by signatures in transport and in crystal vibrational frequencies. Several of the symmetry breaking signatures drop to the $n = 4$ line at dopings lower than $p < 0.085$.

For this line only we omitted data sets which, compared to their linear regressions, showed a scatter of more than 10 to 15 K.

- (a) Zhang, 2018.²⁷ Muon spin relaxation. At temperatures below this temperature the spin relaxation reflects the existence of a slowly fluctuating magnetic field consistent with the intra unit cell order seen by neutron scattering, while above this temperature the field is absent. The entirety of this data is contested by Ref. 93 and a reply to that is contained within Ref. 27.
- (b) Sato, 2017.²⁹ Torque magnetometry measurements of the anisotropic susceptibility. Above this temperature the anisotropy is a linearly increasing function of temperature, while below this temperature it begins increasing as temperature decreases. This signals that at the pseudogap a new contribution to nematic order is added.
- (c) Zhao, 2016.²⁸ Linear and $n = 2$ line optical anisotropy. Below this temperature the $n = 2$ line appears, signaling loss of inversion and C_2 two-fold rotation symmetries. This is a stronger symmetry breaking than either nematic order or orthorhombic symmetry.
- (d) Zhao, 2016, analyzes Lubashevsky, 2014.^{28,41} Optical birefringence. The temperature reported here marks the onset of a polarized signal seen at lower temperatures, which signals loss of both mirror and C_4 four-fold rotation symmetries.
- (e) Sidis-Bourges, 2006-2015.^{31-34,37,49} Polarized neutron scattering showing the onset of intra unit cell order, i.e. time reversal symmetry breaking while retaining lattice translational symmetry. Thirteen points from six different papers. The lowest doping data point, at $p = 0.08$, $T = 170$ K, lies near the $n = 4$ line (about 13 K higher, within the published error bars of ± 30 K), while the other twelve points at higher dopings lie on the $n = 2$ line. We omit this because the data set shows a scatter (compared to its linear regression, and not including the $p = 0.08$ data point) of 30 K, which is above our cutoff.
- (f) Daou, 2018/2010, analyzes Ando, 2004.^{10,17,35} Resistivity. The temperature reported here marks a break from the linear signal seen at higher temperatures. We omit the $p = 0.18$ data point on a specially irradiated sample in Ref. 17.
- (g) Arpaia, 2018.³⁶ Thin film on an MgO substrate. Resistivity. The temperature reported here marks a transition to linearity at higher temperatures.

- (h) Arpaia, 2018.³⁶ Thin film on an SrTiO₃ substrate. Resistivity. The temperature reported here marks a transition to linearity at higher temperatures.
 - (i) Alloul, 2010.³⁹ Resistivity. The temperature measured here marks a transition to the linear resistivity seen at higher temperatures. We omit the $p = 0.169$ data point because the sample has been irradiated to produce more disorder.
 - (j) Wang, 2017.⁴⁰ Resistivity. The temperature recorded here marks the transition to quadratic behavior at low temperatures.
 - (k) Kabanov, 1999.³⁸ Thin films on MgO and SrTiO₃. Photoinduced transmission. The temperature measured here marks the end of a low temperature plateau in $\delta T/T$, where T is the photoinduced transmission signal. We omit this because the data shows a scatter (compared to its linear regression) of 30 to 40 K, which is above our cutoff.
 - (l) Leridon, 2009.³⁰ First derivative of the magnetic susceptibility with respect to temperature. At temperatures above this temperature the derivative is a decreasing function of T , while at lower temperatures it reverses its behavior and begins decreasing as T is reduced. We omit this data set because the data shows a scatter (compared to its linear regression) of 30 to 40 K, which is above our cutoff.
 - (m) Shekhter, 2013.²⁶ Resonant ultrasound spectroscopy measuring crystal resonance frequencies. At this temperature a sharp anomaly is seen in the resonance frequency and its slope changes abruptly. The width of the anomaly is 3 K, which is far sharper than any other data set on the pseudogap.
It is worth noting that, unlike the other pseudogap signatures discussed in this article which focus on electronic response, resonant ultrasound spectroscopy is a probe of ionic motion. As such it belongs to the extensive cuprate literature on mechanically-oriented observables such as internal friction, sound velocity, lattice constants, thermal expansivity, oxygen movement, thermal history dependence, and the like.^{52,71} It is extremely well attested that these observables reveal many distinct anomalies and phase transitions in the temperature range between T_c and room temperature. These features, their dependence on doping, and their qualitative behavior are not yet well understood. In this connection Ref. 94 has contested Ref. 26 's pseudogap data in its entirety.
3. $n = 3$ line: In YBCO the $n = 3$ line is marked by time reversal symmetry breaking, onset of a spin resonance, and a new contribution to nematic order as seen in transport.
- (a) Kapitulnik, 2009.⁴³ This temperature marks the onset of the Kerr effect, signaling time reversal symmetry breaking. We omit the data point at $p = 0.156$ because it has an enormous 87 K error bar.
 - (b) Xia, 2008.⁹⁵ Polar Kerr effect. This temperature marks the onset of the Kerr effect, signalling time reversal symmetry breaking. They also find hysteresis at these temperatures, up to room temperature, indicating that time reversal symmetry breaking occurs also up to room temperature. We omit this data set because three out of four data points are repeated in⁴³ by the same authors.
 - (c) Dai, 1999.⁴² Neutron scattering. The temperatures recorded here mark the onset of a magnetic resonance which is measured by integrating the magnetic structure factor over momentum and frequency.
 - (d) Cyr-Choiniere, 2015.⁴⁴ Nematic component of the Nernst effect. The temperature recorded here marks a transition from steeply decreasing behavior (at low T) to slowly increasing linear behavior (at higher T). The authors argue that this marks the onset of a new contribution to the nematicity, and that this contribution is distinct from the nematicity at higher dopings which may be associated with charge density waves.
 - (e) Cyr - Choiniere, 2015, analyzes Ando, 2004.^{10,44} Nematic component of the resistivity. They plot the ratio ρ_a/ρ_b , where ρ_a and ρ_b are measured along two different axis. The temperature recorded here marks a transition from steeply decreasing behavior (at low T) to slowly increasing linear behavior (at higher T). The authors argue that this marks the onset of a new contribution to the nematicity, and that this contribution is distinct from the nematicity at higher dopings which may be associated with charge density waves.
 - (f) Cyr - Choiniere, 2015.⁴⁴ Nematic component of the resistivity. They plot the ratio ρ_a/ρ_b , where ρ_a and ρ_b are measured along two different axis. The temperature recorded here marks a transition from a steeply decreasing behavior (at low T) to slowly increasing behavior (at higher T). The authors argue that this marks the onset of a new contribution to the nematicity, and that this contribution is distinct from the nematicity at higher dopings which may be associated with charge density waves.

- (g) Wuyts, 1996.⁴⁵ Resistivity. They take the derivative of the resistivity with respect to temperature, find a peak in the derivative, and the peak position is the temperature recorded here. They originally multiplied by two and we remove that factor.
4. $n = 4$ line: In YBCO the extent of the $n = 4$ line, from $p = 0.053$ to $p = 0.142$, is attested to by three transport data sets.
- (a) Arpaia, 2018.³⁶ Thin film on an MgO substrate. Resistivity. The temperature reported here marks a transition from quadratic at lower temperatures. Data from $p = 0.053$ to $p = 0.142$.
- (b) Arpaia, 2018.³⁶ Thin film on an SrTiO₃ substrate. Resistivity. The temperature reported here marks a transition from quadratic at lower temperatures. Data from $p = 0.067$ to $p = 0.140$.
- (c) LeBouef, 2011, analyzes Segawa, 2004.^{46,47} Hall resistance. This temperature records the point where the second derivative of the Hall resistance changes sign. Data from $p = 0.055$ to $p = 0.119$.

At low dopings from $p = 0.052$ to $p = 0.082$ the $n = 4$ line is augmented by intra unit cell order, spontaneous magnetic fields, and new nematic order. At higher dopings similar signals are seen on the $n = 2$ line.

- (a) Haug, 2010.⁴⁸ Neutron scattering. The temperature reported here marks onset of anisotropy in a neutron scattering triple-axis experiment. This is a sign of nematic order, and is called an electronic liquid crystal.
- (b) Baledent, 2011.⁴⁹ Polarized neutron scattering showing the onset of intra unit cell order, i.e. time reversal symmetry breaking while retaining lattice translational symmetry. The lowest doping data point, at $p = 0.08$, $T = 170$ K, lies near the $n = 4$ line (about 13 K higher, within the published error bars of ± 30 K).
- (c) Sonier, 2001.⁵⁰ Muon spin relaxation. This is the extinction temperature of a signal that indicates the presence of small spontaneous magnetic fields. Two data points. The first lies on the $n = 4$ line. We omit the second data point, which lies about 35 K below the $n = 4$ line, well outside the experimental error bars of ± 10 K, and close to the three dimensional charge density waves⁹⁶.
5. Other Data Sets:
- (a) Arpaia, 2018.³⁶ Thin film on an MgO substrate. Resistivity. The temperature reported

here marks a transition to quadratic at higher temperatures. We omit this data from the linear regressions because it clearly has two parts, one at lower doping which decreases very steeply until it hits the superconducting doping, and a second part which follows the superconducting dome.

- (b) Arpaia, 2018.³⁶ Thin film on an SrTiO₃ substrate. Resistivity. The temperature reported here marks a transition to quadratic at higher temperatures.
6. Superconducting T_c , Neel temperature, and charge density waves:
- (a) Coneri, 2010.⁹⁷ Neel temperature measured with muon spin rotation.
- (b) Coneri, 2010.⁹⁷ T_c measured with muon spin rotation.
- (c) Liang, 2006.⁵³ T_c .
- (d) Laliberte, 2018.⁹⁶ Sound velocity measurements of 3-D charge density wave order. We omit the $T = 0$ data points at either side of the dome.
7. Omitted Data Sets:
- (a) Hinkov, 2008.⁹⁸ Neutron scattering. Polarized neutron scattering showing the onset of intra unit cell order, i.e. time reversal symmetry breaking while retaining lattice translational symmetry. We omit this data point because it seems to have been revised from $T = 150$ K to $T = 170$ K in Ref. 49 by the same authors..
- (b) Cyr-Choiniere, 2018 and Daou, 2010.^{17,35} Nernst effect. The temperature reported here marks a break from the linear signal seen at higher temperatures. In³⁵ it is shown that this temperature is the point where anisotropy in the Nernst coefficient is extinguished, at $p = 0.12, 0.13, 0.15, 0.18$. The authors argue that this anisotropy is caused by rotational symmetry breaking in the copper oxide planes as opposed to the oxygen chains. Ref. 44 by the same authors, five years later, re-evaluates the data, and says that the Nernst anisotropy seen in Ref. 35 "is more likely to be caused by CDW modulations" instead of the pseudogap. In other words, although they saw the beginning of a slight rise in the Nernst anisotropy at the pseudogap temperature, the real rise doesn't occur until near the lower temperatures where CDW order is observed using X-ray diffraction. Ref. 44 is an effort to sort out where the new nematicity begins. We omit this data set because the data shows a scatter (compared to its linear regression) of 15 to 20 K, which is above our cutoff for the $n = 1$ line.

This data set cuts across the $n = 1$ and $n = 2$ lines and is rather flat.

- (c) Goto, 1996.⁹⁹ Nuclear magnetic resonance. The temperature reported here marks a peak in the signal. This data set is very flat and cuts through the $n = 2$ and $n = 3$ lines. It roughly coincides with X-ray scattering data on short-range charge density wave order from Ref. 100.

- (d) Cooper, 1996.¹⁰¹ Several pseudogap temperature data sets are reported in Figure 30. This data is omitted because we don't understand where it came from, and also because it seems that the thermoelectric power data in Figure 30 (which runs up to 600 K) was derived from data in Figure 28b, which has a temperature cutoff of 300 K.

* Electronic address: vincent@sacksteder.com

- ¹ D. C. Johnston, Phys. Rev. Lett. **62**, 957 (1989), URL <https://link.aps.org/doi/10.1103/PhysRevLett.62.957>.
- ² R. Yoshizaki, N. Ishikawa, H. Sawada, E. Kita, and A. Tasaki, Physica C: Superconductivity **166**, 417 (1990).
- ³ M. R. Norman, D. Pines, and C. Kallin, Advances in Physics **54**, 715 (2005).
- ⁴ I. M. Vishik, Reports on Progress in Physics **81**, 062501 (2018).
- ⁵ E. Fradkin, S. A. Kivelson, and J. M. Tranquada, Rev. Mod. Phys. **87**, 457 (2015), URL <https://link.aps.org/doi/10.1103/RevModPhys.87.457>.
- ⁶ B. Keimer, S. A. Kivelson, M. R. Norman, S. Uchida, and J. Zaanen, Nature **518**, 179 (2015).
- ⁷ T. Nakano, M. Oda, C. Manabe, N. Momono, Y. Miura, and M. Ido, Phys. Rev. B **49**, 16000 (1994), URL <https://link.aps.org/doi/10.1103/PhysRevB.49.16000>.
- ⁸ J. S. Kim, B. H. Kim, D. C. Kim, and Y. W. Park, Journal of superconductivity **17**, 151 (2004).
- ⁹ H. Takagi, R. J. Cava, M. Marezio, B. Batlogg, J. J. Krajewski, W. F. Peck, P. Bordet, and D. E. Cox, Phys. Rev. Lett. **68**, 3777 (1992), URL <https://link.aps.org/doi/10.1103/PhysRevLett.68.3777>.
- ¹⁰ Y. Ando, S. Komiya, K. Segawa, S. Ono, and Y. Kurita, Phys. Rev. Lett. **93**, 267001 (2004), URL <https://link.aps.org/doi/10.1103/PhysRevLett.93.267001>.
- ¹¹ K. Yamada, C. H. Lee, K. Kurahashi, J. Wada, S. Wakimoto, S. Ueki, H. Kimura, Y. Endoh, S. Hosoya, G. Shirane, et al., Phys. Rev. B **57**, 6165 (1998), URL <https://link.aps.org/doi/10.1103/PhysRevB.57.6165>.
- ¹² B. Keimer, N. Belk, R. J. Birgeneau, A. Cassanho, C. Y. Chen, M. Greven, M. A. Kastner, A. Aharony, Y. Endoh, R. W. Erwin, et al., Phys. Rev. B **46**, 14034 (1992), URL <https://link.aps.org/doi/10.1103/PhysRevB.46.14034>.
- ¹³ T. Yoshida, M. Hashimoto, S. Ideta, A. Fujimori, K. Tanaka, N. Mannella, Z. Hussain, Z.-X. Shen, M. Kubota, K. Ono, et al., Phys. Rev. Lett. **103**, 037004 (2009), URL <https://link.aps.org/doi/10.1103/PhysRevLett.103.037004>.
- ¹⁴ M. Hashimoto, T. Yoshida, K. Tanaka, A. Fujimori, M. Okusawa, S. Wakimoto, K. Yamada, T. Kakeshita, H. Eisaki, and S. Uchida, Phys. Rev. B **75**, 140503 (2007), URL <https://link.aps.org/doi/10.1103/PhysRevB.75.140503>.
- ¹⁵ C. E. Matt, C. G. Fatuzzo, Y. Sassa, M. Månsson, S. Fatale, V. Bitetta, X. Shi, S. Pailhès, M. H. Berntsen, T. Kurosawa, et al., Phys. Rev. B **92**, 134524 (2015), URL <https://link.aps.org/doi/10.1103/PhysRevB.92.134524>.
- ¹⁶ T. Fujii, T. Matsushima, T. Maruoka, and A. Asamitsu, Physica C: Superconductivity and its Applications **470**, S21 (2010), ISSN 0921-4534, proceedings of the 9th International Conference on Materials and Mechanisms of Superconductivity, URL <http://www.sciencedirect.com/science/article/pii/S0921453409009186>.
- ¹⁷ O. Cyr-Choinière, R. Daou, F. Laliberté, C. Collignon, S. Badoux, D. LeBoeuf, J. Chang, B. J. Ramshaw, D. A. Bonn, W. N. Hardy, et al., Phys. Rev. B **97**, 064502 (2018), URL <https://link.aps.org/doi/10.1103/PhysRevB.97.064502>.
- ¹⁸ Z. A. Xu, N. P. Ong, Y. Wang, T. Kakeshita, and S. Uchida, Nature **406**, 486 (2000).
- ¹⁹ Y. Wang, Z. A. Xu, T. Kakeshita, S. Uchida, S. Ono, Y. Ando, and N. P. Ong, Phys. Rev. B **64**, 224519 (2001), URL <https://link.aps.org/doi/10.1103/PhysRevB.64.224519>.
- ²⁰ Y. Itoh, T. Machi, N. Koshizuka, M. Murakami, H. Yamagata, and M. Matsumura, Phys. Rev. B **69**, 184503 (2004), URL <https://link.aps.org/doi/10.1103/PhysRevB.69.184503>.
- ²¹ C. Collignon, S. Badoux, S. A. A. Afshar, B. Michon, F. Laliberté, O. Cyr-Choinière, J.-S. Zhou, S. Licciardello, S. Wiedmann, N. Doiron-Leyraud, et al., Phys. Rev. B **95**, 224517 (2017), URL <https://link.aps.org/doi/10.1103/PhysRevB.95.224517>.
- ²² V. Balédent, B. Fauqué, Y. Sidis, N. B. Christensen, S. Pailhès, K. Conder, E. Pomjakushina, J. Mesot, and P. Bourges, Phys. Rev. Lett. **105**, 027004 (2010), URL <https://link.aps.org/doi/10.1103/PhysRevLett.105.027004>.
- ²³ Z. A. Xu, N. P. Ong, T. Kakeshita, H. Eisaki, and S. Uchida, Physica C: Superconductivity **341**, 1711 (2000).
- ²⁴ T. Matsuzaki, N. Momono, M. Oda, and M. Ido, Journal of the Physical Society of Japan **73**, 2232 (2004).
- ²⁵ N. Doiron-Leyraud, P. Auban-Senzier, S. R. de Cotret, A. Sedeki, C. Bourbonnais, D. Jerome, K. Bechgaard, and L. Taillefer, arXiv preprint arXiv:0905.0964 (2009).
- ²⁶ A. Shekhter, B. J. Ramshaw, R. Liang, W. N. Hardy, D. A. Bonn, F. F. Balakirev, R. D. McDonald, J. B. Betts, S. C. Riggs, and A. Migliori, Nature **498**, 75 (2013).
- ²⁷ J. Zhang, Z. Ding, C. Tan, K. Huang, O. O. Bernal, P.-C. Ho, G. D. Morris, A. D. Hillier, P. K. Biswas, S. P. Cottrell, et al., Science advances **4**, eaao5235 (2018).
- ²⁸ L. Zhao, C. A. Belvin, R. Liang, D. A. Bonn, W. N. Hardy, N. P. Armitage, and D. Hsieh, Nature Physics **13**, 250

- (2017).
- ²⁹ Y. Sato, S. Kasahara, H. Murayama, Y. Kasahara, E.-G. Moon, T. Nishizaki, T. Loew, J. Porras, B. Keimer, T. Shibauchi, et al., *Nature Physics* **13**, 1074 (2017).
 - ³⁰ B. Leridon, P. Monod, D. Colson, and A. Forget, *EPL (Europhysics Letters)* **87**, 17011 (2009).
 - ³¹ B. Fauqué, Y. Sidis, V. Hinkov, S. Pailhès, C. T. Lin, X. Chaud, and P. Bourges, *Phys. Rev. Lett.* **96**, 197001 (2006), URL <https://link.aps.org/doi/10.1103/PhysRevLett.96.197001>.
 - ³² L. Mangin-Thro, Y. Li, Y. Sidis, and P. Bourges, *Phys. Rev. Lett.* **118**, 097003 (2017), URL <https://link.aps.org/doi/10.1103/PhysRevLett.118.097003>.
 - ³³ H. A. Mook, Y. Sidis, B. Fauqué, V. Balédent, and P. Bourges, *Phys. Rev. B* **78**, 020506 (2008), URL <https://link.aps.org/doi/10.1103/PhysRevB.78.020506>.
 - ³⁴ L. Mangin-Thro, Y. Sidis, A. Wildes, and P. Bourges, *Nature communications* **6**, 7705 (2015).
 - ³⁵ R. Daou, J. Chang, D. LeBoeuf, O. Cyr-Choiniere, F. Laliberté, N. Doiron-Leyraud, B. J. Ramshaw, R. Liang, D. A. Bonn, W. N. Hardy, et al., *Nature* **463**, 519 (2010).
 - ³⁶ R. Arpaia, E. Andersson, E. Trabaldo, T. Bauch, and F. Lombardi, *Phys. Rev. Materials* **2**, 024804 (2018), URL <https://link.aps.org/doi/10.1103/PhysRevMaterials.2.024804>.
 - ³⁷ Y. Sidis, B. Fauqué, V. Aji, and P. Bourges, *Physica B: Condensed Matter* **397**, 1 (2007).
 - ³⁸ V. V. Kabanov, J. Demsar, B. Podobnik, and D. Mihailovic, *Phys. Rev. B* **59**, 1497 (1999), URL <https://link.aps.org/doi/10.1103/PhysRevB.59.1497>.
 - ³⁹ H. Alloul, F. Rullier-Albenque, B. Vignolle, D. Colson, and A. Forget, *EPL (Europhysics Letters)* **91**, 37005 (2010).
 - ⁴⁰ Y. Wang and J. Zhang, arXiv preprint arXiv:1711.07402 (2017).
 - ⁴¹ Y. Lubashevsky, L. Pan, T. Kirzhner, G. Koren, and N. P. Armitage, *Phys. Rev. Lett.* **112**, 147001 (2014), URL <https://link.aps.org/doi/10.1103/PhysRevLett.112.147001>.
 - ⁴² P. Dai, H. A. Mook, S. M. Hayden, G. Aeppli, T. G. Perring, R. D. Hunt, and F. Doğan, *Science* **284**, 1344 (1999).
 - ⁴³ A. Kapitulnik, J. Xia, E. Schemm, and A. Palevski, *New Journal of Physics* **11**, 055060 (2009).
 - ⁴⁴ O. Cyr-Choinière, G. Grissonnanche, S. Badoux, J. Day, D. A. Bonn, W. N. Hardy, R. Liang, N. Doiron-Leyraud, and L. Taillefer, *Phys. Rev. B* **92**, 224502 (2015), URL <https://link.aps.org/doi/10.1103/PhysRevB.92.224502>.
 - ⁴⁵ B. Wuyts, V. V. Moshchalkov, and Y. Bruynseraede, *Phys. Rev. B* **53**, 9418 (1996), URL <https://link.aps.org/doi/10.1103/PhysRevB.53.9418>.
 - ⁴⁶ D. LeBoeuf, N. Doiron-Leyraud, B. Vignolle, M. Sutherland, B. J. Ramshaw, J. Levallois, R. Daou, F. Laliberté, O. Cyr-Choinière, J. Chang, et al., *Phys. Rev. B* **83**, 054506 (2011), URL <https://link.aps.org/doi/10.1103/PhysRevB.83.054506>.
 - ⁴⁷ K. Segawa and Y. Ando, *Phys. Rev. B* **69**, 104521 (2004), URL <https://link.aps.org/doi/10.1103/PhysRevB.69.104521>.
 - ⁴⁸ D. Haug, V. Hinkov, Y. Sidis, P. Bourges, N. B. Christensen, A. Ivanov, T. Keller, C. Lin, and B. Keimer, *New Journal of Physics* **12**, 105006 (2010).
 - ⁴⁹ V. Balédent, D. Haug, Y. Sidis, V. Hinkov, C. T. Lin, and P. Bourges, *Phys. Rev. B* **83**, 104504 (2011), URL <https://link.aps.org/doi/10.1103/PhysRevB.83.104504>.
 - ⁵⁰ J. E. Sonier, J. H. Brewer, R. F. Kiefl, R. I. Miller, G. D. Morris, C. E. Stronach, J. S. Gardner, S. R. Dunsiger, D. A. Bonn, W. N. Hardy, et al., *Science* **292**, 1692 (2001).
 - ⁵¹ A. N. Lavrov, *Physics Letters A* **168**, 71 (1992).
 - ⁵² P. Nagel, V. Pasler, C. Meingast, A. I. Rykov, and S. Tajima, *Phys. Rev. Lett.* **85**, 2376 (2000), URL <https://link.aps.org/doi/10.1103/PhysRevLett.85.2376>.
 - ⁵³ R. Liang, D. A. Bonn, and W. N. Hardy, *Phys. Rev. B* **73**, 180505 (2006), URL <https://link.aps.org/doi/10.1103/PhysRevB.73.180505>.
 - ⁵⁴ R. A. Cooper, Y. Wang, B. Vignolle, O. J. Lipscombe, S. M. Hayden, Y. Tanabe, T. Adachi, Y. Koike, M. Nohara, H. Takagi, et al., *Science* **323**, 603 (2009).
 - ⁵⁵ I. M. Hayes, R. D. McDonald, N. P. Breznay, T. Helm, P. J. W. Moll, M. Wartenbe, A. Shekhter, and J. G. Analytis, *Nature Physics* **12**, 916 (2016).
 - ⁵⁶ P. Giraldo-Gallo, J. A. Galvis, Z. Stegen, K. A. Modic, F. F. Balakirev, J. B. Betts, X. Lian, C. Moir, S. C. Riggs, J. Wu, et al., arXiv preprint arXiv:1705.05806 (2017).
 - ⁵⁷ V. Sacksteder, arXiv preprint arXiv:1801.02663 (2018).
 - ⁵⁸ Y. J. Uemura, G. M. Luke, B. J. Sternlieb, J. H. Brewer, J. F. Carolan, W. N. Hardy, R. Kadono, J. R. Kempton, R. F. Kiefl, S. R. Kreitzman, et al., *Phys. Rev. Lett.* **62**, 2317 (1989), URL <https://link.aps.org/doi/10.1103/PhysRevLett.62.2317>.
 - ⁵⁹ I. Božović, X. He, J. Wu, and A. T. Bollinger, *Nature* **536**, 309 (2016).
 - ⁶⁰ S. Ohsugi, Y. Kitaoka, K. Ishida, and K. Asayama, *Journal of the Physical Society of Japan* **60**, 2351 (1991).
 - ⁶¹ M. Hashimoto, T. Yoshida, K. Tanaka, A. Fujimori, M. Okusawa, S. Wakimoto, K. Yamada, T. Kakeshita, H. Eisaki, and S. Uchida, *Phys. Rev. B* **79**, 140502 (2009), URL <https://link.aps.org/doi/10.1103/PhysRevB.79.140502>.
 - ⁶² U. Chatterjee, D. Ai, J. Zhao, S. Rosenkranz, A. Kaminski, H. Raffy, Z. Li, K. Kadowaki, M. Randeria, M. R. Norman, et al., *Proceedings of the National Academy of Sciences* **108**, 9346 (2011).
 - ⁶³ R. Kumar, S. Singh, and S. Nair, arXiv preprint arXiv:1801.03768 (2018).
 - ⁶⁴ G. P. Mikitik and Y. V. Sharlai, *Phys. Rev. Lett.* **82**, 2147 (1999), URL <https://link.aps.org/doi/10.1103/PhysRevLett.82.2147>.
 - ⁶⁵ D. Xu, J. Qi, J. Liu, V. Sacksteder, X. C. Xie, and H. Jiang, *Phys. Rev. B* **85**, 195140 (2012).
 - ⁶⁶ J. Wu, A. T. Bollinger, X. He, and I. Božović, *Nature* **547**, 432 (2017).
 - ⁶⁷ N. Hussey, R. Cooper, X. Xu, Y. Wang, I. Mouzopoulou, B. Vignolle, and C. Proust, *Philosophical Transactions of the Royal Society of London A: Mathematical, Physical and Engineering Sciences* **369**, 1626 (2011).
 - ⁶⁸ A. Ino, T. Mizokawa, K. Kobayashi, A. Fujimori, T. Sasagawa, T. Kimura, K. Kishio, K. Tamasaku, H. Eisaki, and S. Uchida, *Phys. Rev. Lett.* **81**, 2124 (1998), URL <https://link.aps.org/doi/10.1103/PhysRevLett.81.2124>.
 - ⁶⁹ C. Panagopoulos, M. Majoros, T. Nishizaki, and H. Iwasaki, *Phys. Rev. Lett.* **96**, 047002 (2006), URL <https://link.aps.org/doi/10.1103/PhysRevLett.96.047002>.
 - ⁷⁰ C. Panagopoulos, M. Majoros, and A. P. Petrović, *Phys. Rev. B* **69**, 144508 (2004), URL <https://link.aps.org/>

- doi/10.1103/PhysRevB.69.144508.
- ⁷¹ J. Dominec, *Superconductor Science and Technology* **6**, 153 (1993).
- ⁷² F. Laliberté, W. Tabis, S. Badoux, B. Vignolle, D. Destraz, N. Momono, T. Kurosawa, K. Yamada, H. Takagi, N. Doiron-Leyraud, et al., arXiv preprint arXiv:1606.04491 (2016).
- ⁷³ O. Cyr-Choiniere, R. Daou, F. Laliberté, D. LeBoeuf, N. Doiron-Leyraud, J. Chang, J.-Q. Yan, J.-G. Cheng, J.-S. Zhou, J. B. Goodenough, et al., *Nature* **458**, 743 (2009).
- ⁷⁴ N. Ichikawa, S. Uchida, J. M. Tranquada, T. Niemöller, P. M. Gehring, S.-H. Lee, and J. R. Schneider, *Phys. Rev. Lett.* **85**, 1738 (2000), URL <https://link.aps.org/doi/10.1103/PhysRevLett.85.1738>.
- ⁷⁵ N. Momono, M. Ido, T. Nakano, M. Oda, Y. Okajima, and K. Yamaya, *Physica C: Superconductivity* **233**, 395 (1994).
- ⁷⁶ B. Keimer, A. Aharony, A. Auerbach, R. J. Birgeneau, A. Cassanho, Y. Endoh, R. W. Erwin, M. A. Kastner, and G. Shirane, *Phys. Rev. B* **45**, 7430 (1992), URL <https://link.aps.org/doi/10.1103/PhysRevB.45.7430>.
- ⁷⁷ M. Matsuda, M. Fujita, K. Yamada, R. J. Birgeneau, Y. Endoh, and G. Shirane, *Phys. Rev. B* **65**, 134515 (2002), URL <https://link.aps.org/doi/10.1103/PhysRevB.65.134515>.
- ⁷⁸ C. Niedermayer, C. Bernhard, T. Blasius, A. Golnik, A. Moodenbaugh, and J. I. Budnick, *Phys. Rev. Lett.* **80**, 3843 (1998), URL <https://link.aps.org/doi/10.1103/PhysRevLett.80.3843>.
- ⁷⁹ M. Majoros, C. Panagopoulos, T. Nishizaki, and H. Iwasaki, *Phys. Rev. B* **72**, 024528 (2005), URL <https://link.aps.org/doi/10.1103/PhysRevB.72.024528>.
- ⁸⁰ M. Oda, H. Matsuki, and M. Ido, *Solid State Communications* **74**, 1321 (1990).
- ⁸¹ M. Oda, T. Ohguro, H. Matsuki, N. Yamada, and M. Ido, *Physical Review B* **41**, 2605 (1990).
- ⁸² M. Oda, T. Nakano, Y. Kamada, and M. Ido, *Physica C: Superconductivity* **183**, 234 (1991).
- ⁸³ N. Momono and M. Ido, *Physica C: Superconductivity* **264**, 311 (1996).
- ⁸⁴ T. Nakano, N. Momono, M. Oda, and M. Ido, *Journal of the Physical Society of Japan* **67**, 2622 (1998).
- ⁸⁵ H. Y. Hwang, B. Batlogg, H. Takagi, H. L. Kao, J. Kwo, R. J. Cava, J. J. Krajewski, and W. F. Peck, *Phys. Rev. Lett.* **72**, 2636 (1994), URL <https://link.aps.org/doi/10.1103/PhysRevLett.72.2636>.
- ⁸⁶ B. Batlogg, H. Y. Hwang, H. Takagi, H. L. Kao, J. Kwo, and R. J. Cava, *Journal of Low Temperature Physics* **95**, 23 (1994).
- ⁸⁷ J. L. Tallon, J. W. Loram, G. V. M. Williams, J. R. Cooper, I. R. Fisher, J. D. Johnson, M. P. Staines, and C. Bernhard, *Physica Status Solidi B* **215**, 531 (1999).
- ⁸⁸ G. S. Boebinger, Y. Ando, A. Passner, T. Kimura, M. Okuya, J. Shimoyama, K. Kishio, K. Tamasaku, N. Ichikawa, and S. Uchida, *Phys. Rev. Lett.* **77**, 5417 (1996), URL <https://link.aps.org/doi/10.1103/PhysRevLett.77.5417>.
- ⁸⁹ T. Takemura, T. Kitajima, T. Sugaya, and I. Terasaki, *Journal of Physics: Condensed Matter* **12**, 6199 (2000).
- ⁹⁰ T. Nishikawa, J. Takeda, and M. Sato, *Journal of the Physical Society of Japan* **63**, 1441 (1994).
- ⁹¹ T. Startseva, T. Timusk, A. V. Puchkov, D. N. Basov, H. A. Mook, M. Okuya, T. Kimura, and K. Kishio, *Phys. Rev. B* **59**, 7184 (1999), URL <https://link.aps.org/doi/10.1103/PhysRevB.59.7184>.
- ⁹² Y. Wang, L. Li, and N. P. Ong, *Phys. Rev. B* **73**, 024510 (2006), URL <https://link.aps.org/doi/10.1103/PhysRevB.73.024510>.
- ⁹³ J. E. Sonier, arXiv preprint arXiv:1706.03023 (2017).
- ⁹⁴ J. Cooper, J. Loram, I. Kokanović, J. Storey, and J. Tallon, *Physical Review B* **89**, 201104 (2014).
- ⁹⁵ J. Xia, E. Schemm, G. Deutscher, S. A. Kivelson, D. A. Bonn, W. N. Hardy, R. Liang, W. Siemons, G. Koster, M. M. Fejer, et al., *Phys. Rev. Lett.* **100**, 127002 (2008), URL <https://link.aps.org/doi/10.1103/PhysRevLett.100.127002>.
- ⁹⁶ F. Laliberté, M. Frachet, S. Benhabib, B. Borgnic, T. Loew, J. Porras, M. Tacon, B. Keimer, S. Wiedmann, C. Proust, et al., *npj Quantum Materials* **3**, 11 (2018).
- ⁹⁷ F. Coneri, S. Sanna, K. Zheng, J. Lord, and R. De Renzi, *Phys. Rev. B* **81**, 104507 (2010), URL <https://link.aps.org/doi/10.1103/PhysRevB.81.104507>.
- ⁹⁸ V. Hinkov, D. Haug, B. Fauqué, P. Bourges, Y. Sidis, A. Ivanov, C. Bernhard, C. Lin, and B. Keimer, *Science* **319**, 597 (2008).
- ⁹⁹ A. Goto, H. Yasuoka, and Y. Ueda, *Journal of the Physical Society of Japan* **65**, 3043 (1996).
- ¹⁰⁰ S. Blanco-Canosa, A. Frano, E. Schierle, J. Porras, T. Loew, M. Minola, M. Bluschke, E. Weschke, B. Keimer, and M. Le Tacon, *Phys. Rev. B* **90**, 054513 (2014), URL <https://link.aps.org/doi/10.1103/PhysRevB.90.054513>.
- ¹⁰¹ J. R. Cooper and J. W. Loram, *Journal de Physique I* **6**, 2237 (1996).
- ¹⁰² We place the intersection at $p = 0.26$, $T = 0$ K and align the second pseudogap line to the experimental data point in¹² at $p = 0$, $T = 515$ K.
- ¹⁰³ We align the $n = 2$ pseudogap line to $p = 0$, $T = 500$ K and $p = 0.215$, $T = 0$.
- ¹⁰⁴ It may be worth noting that at $p = 0$ the $n = 1$ line's temperature $T = 1000$ K, if converted to area A via $\hbar^2 A^{-1}/2m_e = k_B T$, gives an area $A = 158 a_0^2$. This is three times the area of the copper oxide unit cell.
- ¹⁰⁵ Judging from authors' estimates, comparison of data sets to their linear regressions, and comparison between data sets, most data sets show scatters or errors of ± 10 to ± 20 Kelvin. A notable exception is²⁶, which reports that YBCO's $n = 2$ pseudogap line has a width of 3 K. There are also several data sets with exceptionally large scatters of 50 K or more, including three out of four data sets on LSCO's $n = 1$ line and also the thermoelectric power data on LSCO's $n = 2$ line.^{2,7,8} We have not included in our figures three data sets on YBCO's $n = 2$ pseudogap line because their scatters are larger than 15 K^{30,38}, including neutron scattering data revealing intra unit cell order.^{31-34,37,49}